ADVANCED LEVEL-SET BASED MULTIPLE-CELL SEGMENTATION AND TRACKING IN TIME-LAPSE FLUORESCENCE MICROSCOPY IMAGES

Oleh Dzyubachyk, Wiro Niessen and Erik Meijering

Biomedical Imaging Group Rotterdam
Erasmus MC — University Medical Center Rotterdam
Email: o.dzyubachyk@erasmusmc.nl

ABSTRACT

Segmentation and tracking of cells in fluorescence microscopy image sequences is an important task in many biological studies into cell migration as well as intracellular dynamics. The growing size and complexity of biological image data sets precludes manual analysis, and calls for increasingly advanced automatic algorithms that are generic enough to be easily tunable to different applications, yet robust enough to deal with different cell types and strongly varying imaging conditions. Active-contour based algorithms have proven to be very suitable for this purpose but still suffer from several shortcomings that limit their segmentation accuracy and tracking robustness. In addition, these algorithms are generally rather computationally expensive. In this paper, we present an advanced level-set based multiple-cell segmentation and tracking algorithm, which implements seven modifications compared to earlier algorithms that considerably improve its performance. Preliminary experiments on three different time-lapse fluorescence microscopy images demonstrate the potential of the new algorithm.

Index Terms— Fluorescence microscopy, cell segmentation, level sets, Radon transform, cell tracking.

1. INTRODUCTION

Directed cell migration is an important property of number of cell types and one of the central processes in the development and maintenance of a multicellular organism [1]. Analysis of cell motility and morphodynamics under normal and perturbed conditions help to better understand complex regulatory processes within the cell as well as interactions between different cells. The ever growing size and complexity of fluorescence microscopy image data sets poses new challenges to cell segmentation and tracking techniques. In order to keep up with the rapid developments in the field, existing algorithms need improvement with respect to accuracy, robustness, as well as computation time.

Various algorithms have been developed for this purpose during the past few years [2, 3, 4, 5, 6]. In general they can be divided into two categories [7]: algorithms performing segmentation and tracking separately, and algorithms considering segmentation and tracking as one process. Recent literature shows an increasing interest in the latter category, particularly in active-contour based schemes (using snakes or level-sets), as they offer the possibility to better exploit all available spatiotemporal information contained in the image sequences. However, existing algorithms show limited performance when applied to real biological image data, which usually have a very low signal-to-noise ratio and contain many cells that may be in close contact [2]. In addition, such algorithms are relatively computationally expensive in general, which makes them less attractive for the practical use, especially in high-throughput experiments.

In this paper we present an advanced level-set based algorithm for combined segmentation and tracking of multiple cells in fluorescence microscopy image sequences. It implements seven important modifications compared to earlier algorithms [2], which considerably improve its performance in terms of accuracy, robustness, and computation time. First, we present a reformulation of the original framework, which reduces the number of free parameters to be tuned. Then we propose new approaches for algorithm initialization, termination of level-set evolution, separation of touching cells, non-PDE based segmentation, detection and segmentation of newly entering cells, and economical recomputation of parameters. The potential of our modified algorithm is demonstrated by preliminary experiments on three different real fluorescence microscopy image sequences.

2. MULTIPLE-LEVEL-SET FRAMEWORK

In our segmentation and tracking framework, each object (cell or nucleus) is represented by a separate level-set function, ϕ_i, $i = 1, \ldots, n$, where n is the number of objects. Optimal segmentation of each 3D image from a sequence is obtained by minimizing an energy functional, which contains both image-based and smoothness-based components:

$$E(\phi_1, \ldots, \phi_n) = \sum_{i=0}^{n} \iiint_{\Omega_i} - \log p\left(I(\mathbf{x})|\Omega_i\right) dx dy dz$$
$$+ \alpha \cdot \text{Length}(\partial\Omega), \quad (1)$$

where Ω_0 is the background, $\Omega_i = \{\mathbf{x} : \phi_i(\mathbf{x}) > 0\}$, $i = 1, \ldots, n$, are the object regions such that $\Omega = \bigcup_{i=0}^{n} \Omega_i$ is the

image domain, $\partial\Omega$ is the boundary between regions, and α is a positive parameter. $p\left(I(\mathbf{x})|\Omega_i\right)$ is the conditional probability that voxel $\mathbf{x} = (x, y, z)$ with intensity $I(\mathbf{x})$ belongs to region Ω_i [8]. Unlike earlier approaches [2], we assume that its distribution is Gaussian, which allows us to introduce the "internal" energies of the background and objects as

$$e_i = -\log p(I|\Omega_i) = \log \sigma_i^2 + \frac{(I - \mu_i)^2}{\sigma_i^2}, \qquad (2)$$

where μ_i and σ_i denote the mean and the variance of the intensity distribution within region Ω_i, $i = 0, \ldots, n$.

The evolution equation for each level-set function is derived using the variational approach. Applying to (1) the Euler-Lagrange equation results in the following evolution equation for the level-set functions ϕ_i, $i = 1, \ldots, n$:

$$\frac{\partial \phi_i}{\partial t} = \delta_\varepsilon(\phi_i) \left[\alpha \nabla \cdot \frac{\nabla \phi_i}{|\nabla \phi_i|} + e_0 - e_i \right], \qquad (3)$$

where δ_ε denotes the regularized Dirac function. The Euler-Lagrange equations for the parameters describing the Gaussian intensity distributions can be solved directly, giving

$$\mu_0 = \frac{\iiint_\Omega I \prod_{j=1}^n \left(1 - H_\varepsilon(\phi_j)\right) dx dy dz}{\iiint_\Omega \prod_{j=1}^n \left(1 - H_\varepsilon(\phi_j)\right) dx dy dz},$$

$$\sigma_0^2 = \frac{\iiint_\Omega (I - \mu_0)^2 \prod_{j=1}^n \left(1 - H_\varepsilon(\phi_j)\right) dx dy dz}{\iiint_\Omega \prod_{j=1}^n \left(1 - H_\varepsilon(\phi_j)\right) dx dy dz},$$

$$\mu_i = \frac{\iiint_\Omega I H_\varepsilon(\phi_i) dx dy dz}{\iiint_\Omega H_\varepsilon(\phi_i) dx dy dz} \quad \text{for } i = 1, \ldots, n, \text{with}$$

$$\sigma_i^2 = \frac{\iiint_\Omega (I - \mu_i)^2 H_\varepsilon(\phi_i) dx dy dz}{\iiint_\Omega H_\varepsilon(\phi_i) dx dy dz}, \qquad (4)$$

where H_ε is the regularized Heaviside step function. Segmentation proceeds by evolving each level-set function according to (3), starting from its initial position. Tracking is accomplished by using the final level-set positions in a given image in the sequence as initial positions for the next.

3. ALGORITHM IMPROVEMENTS

In addition to using a reformulation of the multiple-level-set based cell tracking framework, as described above, we propose six further improvements, which make our algorithm more accurate, robust, and efficient.

Watershed Based Initialization. The first image of a sequence can be segmented by using one level-set function and splitting the function based on the number of connected components. Since tracking depends critically on the outcome of this step, each cell in the image must be detected precisely. To resolve ambiguous cases of possibly lumped cells, we subsequently apply the watershed transform, which allows separating closely positioned cells and automatically detects connected components. Since standard watershed segmentation tends to produce oversegmentation [3], we combine it with region merging based on the flood-level threshold.

Sign-Change Based Stopping Criterion. The stopping criterion for level-set evolution (3) is a critical factor in trading off segmentation accuracy and computational efficiency [9]. We developed a criterion based on the number of sign changes (indicating inclusion or exclusion) of voxels in a narrow band around the zero-level of the level-set function during a number of consecutive iterations. Optimal performance is obtained by disregarding sign changes of voxels directly bordering the zero-level from both sides, as it is often not possible to determine with great certainty whether these voxels belong to the cell or to the background.

Radon-Transform Based Cell Separation. Concurrent evolution of multiple level-set functions entails the risk that the surface corresponding to one of the cells captures a (part of a) closely neighboring cell. In [2] this was accounted for by using an energy term that penalizes overlaps. However, this does not always result in correct location of the surfaces, since it is not based on the image data, implying that there is no favored position for the cell boundary. Adding a volume conservation constraint [2] leads to problems in handling cell divisions. Instead, in our algorithm, we use the Radon transform to perform cell separation. A similar idea has been used previously for segmenting mammospheres [10]. For each pair of approaching cell surfaces, we calculate the Radon transform of the intensity distribution in a window around the union of the two cell regions, and find the local minimum in the transform domain corresponding to the plane that (i) separates two cell markers (the centers of mass), and (ii) has the smallest cross section. Each of the two evolving level-set surfaces is constrained to stay on one side of the plane.

Non-PDE Based Segmentation. For obtaining a good initial approximation when segmenting the first image in a sequence using one level-set function [2], and also for detecting cells entering the field of view, a non-PDE based segmentation scheme [11] is used in our algorithm. However, instead of computing (1) several iterations with $\alpha \neq 0$ and then several iterations with $\alpha = 0$ [2], we perform voxel swapping based on the image-based energy only, followed by voxel swapping based on the smoothness-based energy term only, within one iteration. This approach does not involve the free parameter α, thereby increasing the robustness of the scheme. In addition, it allows the use of a simpler convergence condition,

based on checking the number of voxels that changed sign, thereby considerably reducing the computational cost. To further speed up the non-PDE based scheme, we approximate the surface area with a cut metric [12].

Segmentation of Entering Cells. An important aspect of cell tracking is the detection of cells entering the field of view. In our algorithm, we deal with this using the following procedure, applied to each image in the sequence. First, we evolve the existing level-sets without considering entering cells. Next, we apply to the image the non-PDE based segmentation scheme described above. From the result of the latter step, we determine possible candidates, being those connected components that are located at the image boundary and do not intersect with any of the existing cells. Finally, for each candidate, we create a level-set function and continue evolution (3), starting from the current positions. Since most cells were already correctly segmented, this process takes relatively little time to converge.

Economical Recomputation of Parameters. Minimization of (1) according to (3) suggests that the parameters (4) should be recalculated after every iteration, which is computationally costly. A possible solution to this problem is to assume that these parameters do not change significantly between two consecutive images in a sequence, and to keep them fixed per image. However, this assumption is not always valid, especially in the case of cell division, where the mean and variance of the intensity distribution in a cell may change drastically from one image to the next. Therefore, we suggest an intermediate solution, by updating the parameters not every iteration, but after a number of iterations.

4. EXPERIMENTAL RESULTS

The performance of the described algorithm was tested on three real 3D microscopy image sequences, with increasing level of difficulty for segmentation and tracking. All images were acquired with a laser-scanning confocal microscope (Zeiss LSM-510) using an oil-immersion objective (Plan-Apochromat 63×/1.4) and a matrix of 512×512 pixels per focal plane (pixel size 190×190nm^2), with 6 focal planes (5μm apart) per image, but different numbers of time frames, and different types of fluorescent labeling.

The first sequence (see Fig. 1), consisting of 85 time frames ($\approx$ 9 min. between images), shows the nuclei of HeLa cells, visualized using histone-based green fluorescent protein (H2B-GFP) labeling, which is characterized by more or less homogeneous fluorescence. Here, the main difficulty is the dramatic change in shape that occurs during cell division, and the fact that the daughter cells often move a considerable distance from the mother cell, violating the preconditions of earlier algorithms [2]. Nevertheless, our algorithm was able to correctly keep track of all nuclei.

The second sequence (see Fig. 2), consisting of 50 time frames ($\approx$ 17 min. between images), shows the nuclei of HeLa cells in which Rad18 proteins (involved in DNA repair) are labeled with yellow fluorescent proteins (YFP). In addition to the problem of cell division, in this case the fluorescence is much less homogeneous, forming clusters of very high intensity values, while other regions may have very low intensities, close to the background level. Also, during division, the mean intensity within a nucleus may drop quite strongly. Despite these difficulties, our algorithm correctly segmented and tracked all cells correctly.

Finally, as a third sequence (see Fig. 3), we used the red channel of the same data set as the second sequence, which shows mCherry-labeled PCNA particles (involved in DNA repair and replication). In this case, not only the nuclei, but sometimes also whole cells are visible, which may be in direct contact. As can be observed from the data, the boundaries between these cells are practically linear, and in all cases our algorithm was able to find the correct separating surface.

5. DISCUSSION

In this paper we have discussed a number of shortcomings of existing level-set based algorithms for multiple-cell segmentation and tracking in fluorescence microscopy, that have a negative effect on the segmentation quality, tracking robustness, as well as time consumption, and we have proposed effective and efficient solutions for each of them. The results of preliminary experiments on real 3D image sequences acquired for different biological studies show that the improved algorithm correctly segments and tracks cells and nuclei of widely varying appearance caused by different fluorescent labelings. In addition, it robustly deals with cases of dividing and touching cells, where previous algorithms failed. We are currently undertaking a thorough validation of the algorithm in the context of several biological studies requiring careful cell motion registration to allow the analysis of intracellular patterns and dynamics.

6. REFERENCES

[1] D. Dormann, C. J. Weijer, "Imaging of cell migration," *EMBO J.*, vol. 25, no. 5, pp. 3480–3493, 2006.

[2] A. Dufour, V. Shinin, S. Tajbakhsh, N. Guillén-Aghion, J.-C. Olivo-Marin, and C. Zimmer, "Segmenting and tracking fluorescent cells in dynamic 3-D microscopy with coupled active surfaces," *IEEE Trans. Image Process.*, vol. 14, no. 9, pp. 1396–1410, 2005.

[3] X. Yang, H. Li, X. Zhou, "Nuclei segmentation using marker-controlled watershed, tracking using mean-shift, and Kalman filter in time-lapse microscopy," *IEEE Trans. Circuits Syst. I-Regul. Pap.*, vol. 53, no. 11, pp. 2405–2414, 2006.

[4] O. Debeir, I. Camby, R. Kiss, P. Van Ham, C. Decaestecker, "A model-based approach for automated in vitro cell tracking and chemotaxis analyses," *Cytometry*, vol. 60A, no. 1, pp. 29–40, 2004.
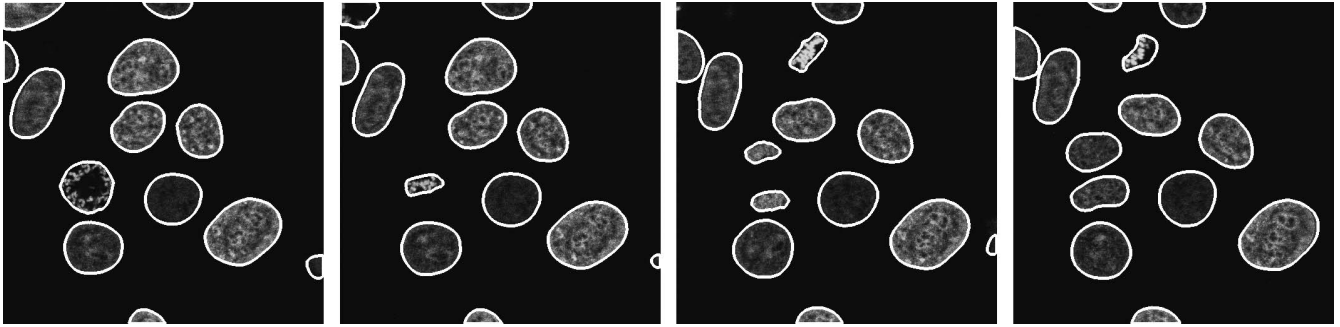
Fig. 1. Sample results of nuclei tracking in the GFP channel of images obtained using the H2B staining. One slice of the 3D image is shown for time steps 12, 16, 28 and 34.
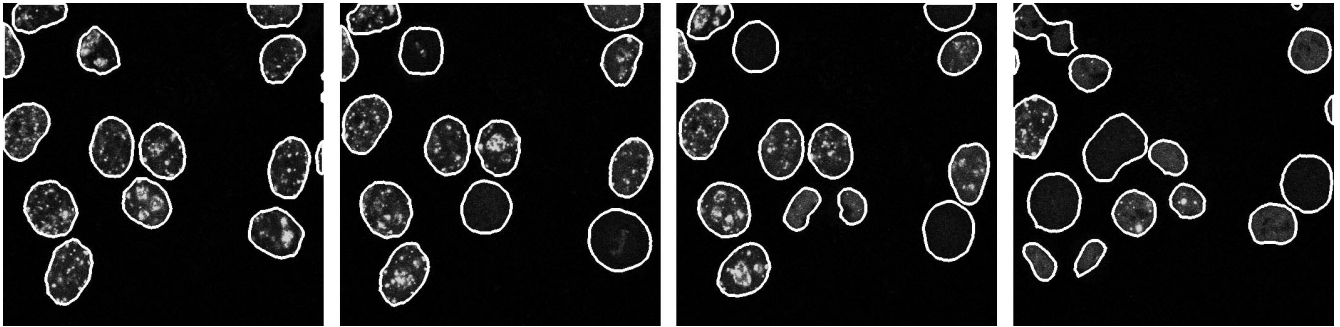

Fig. 2. Sample results of nuclei tracking in the YFP channel of images obtained using the Rad18 staining. One slice of the 3D image is shown for time steps 24, 29, 33 and 44.
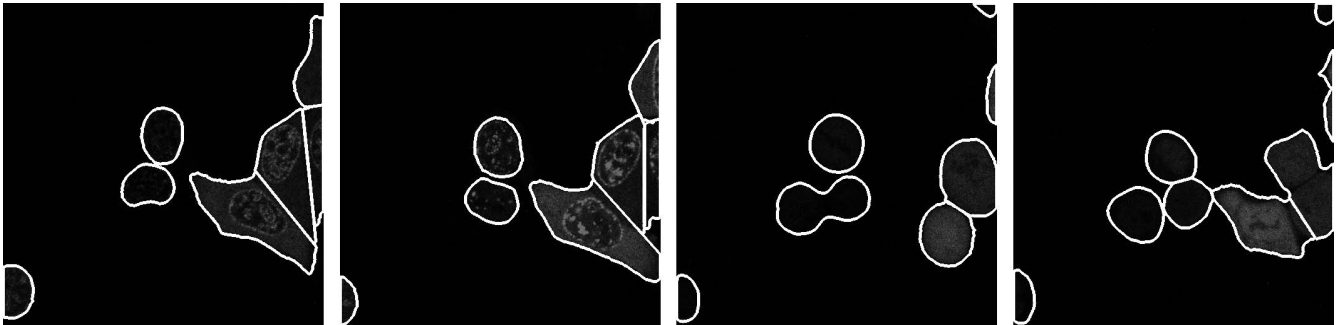

Fig. 3. Sample results of nuclei tracking in the mCherry channel of images obtained using the PCNA staining. One slice of the 3D image is shown for time steps 1, 12, 37 and 50.

[5]   D. P. Mukherjee, N. Ray, S. T. Acton, "Level set analysis for leukocyte detection and tracking," *IEEE Trans. Med. Imaging*, vol. 13, no. 4, pp. 562–572, 2004.

[6]   H. Shen, G. Nelson, S. Kennedy, D. Nelson, J. Johnson, D. Spiller, M. R. H. White, D. B. Kell, "Automatic tracking of biological cells and compartments using particle filters and active contours," *Chemometrics Intell. Lab. Syst.*, vol. 82, nos. 1-2, pp. 276–282, 2006.

[7]   C. Zimmer, B. Zhang, A. Dufour, A. Thébaud, S. Berlemont, V. Meas-Yedid, J.-C. Olivo-Marin, "On the digital trail of mobile cells," *IEEE Signal Process. Mag.*, vol. 23, no. 3, pp. 54–62, 2006.

[8]   M. Rousson, R. Deriche, "A variational framework for active and adaptive segmentation of vector-valued images," *IEEE Workshop on Motion and Video Computing*, pp. 56–62, 2002.

[9]   K. N. Chaudhury, K. R. Ramakrishnan, "Stability and convergence of the level set method in computer vision," *Pattern Recogn. Lett.*, vol. 28, no. 7, pp. 884–893, 2007.

[10]   J. Han, H. Chang, Q. Yang, M.H. Barcellos-Hoff, B. Parvin, "3D segmentation of mammospheres for localization studies," *International Symposium on Visual Computing*, pp. 518–527, 2006.

[11]   B. Song, "Topics in variational PDE image segmentation, inpainting and denoising," PhD thesis, Dept. Math., Univ. California, Los Angeles, USA, 2003.

[12]   Y. Boykov, V. Kolmogorov, "Computing geodesics and minimal surfaces via graph cuts," *International Conference on Computer Vision*, pp. 26–33, 2003.